UC Berkeley
UC Berkeley Previously Published Works

Title
Tunable Carrier Type and Density in Graphene/PbZr0.2Ti0.8O3 Hybrid Structures through Ferroelectric Switching

Permalink
https://escholarship.org/uc/item/84q2k2pk

Journal
Nano Letters, 13(4)

ISSN
1530-6984

Authors
Baeumer, Christoph
Rogers, Steven P
Xu, Ruijuan
et al.

Publication Date
2013-04-10

DOI
10.1021/nl4002052

Peer reviewed

eScholarship.org Powered by the California Digital Library
University of California

NANO LETTERS
Letter
pubs.acs.org/NanoLett

Tunable Carrier Type and Density in Graphene/$PbZr_{0.2}Ti_{0.8}O_3$ Hybrid Structures through Ferroelectric Switching

Christoph Baeumer,[†] Steven P. Rogers,[†] Ruijuan Xu,[†] Lane W. Martin,[*,†] and Moonsub Shim[*,†]

[†]Department of Materials Science and Engineering and Materials Research Laboratory, University of Illinois, Urbana, Illinois 61801, United States

Supporting Information

ABSTRACT: Bidirectional interdependency between graphene doping level and ferroelectric polarization is demonstrated in graphene/$PbZr_{0.2}Ti_{0.8}O_3$ hybrid structures. The polarization of the $PbZr_{0.2}Ti_{0.8}O_3$ can be effectively switched with graphene electrodes and can in turn alter carrier type and density in the graphene. A complete reversal of the current–voltage hysteresis direction is observed in the graphene when external environmental factors are minimized, converting p-type graphene into n-type with an estimated carrier density change as large as $\sim 10^{13}$ cm^{-2}. Nonvolatility and reversibility are also demonstrated.

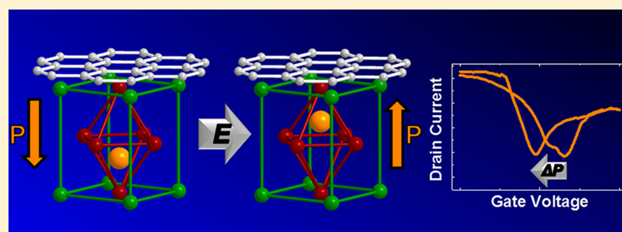

KEYWORDS: *CVD graphene, ferroelectrics, $PbZr_{0.2}Ti_{0.8}O_3$, polarization reversal, interface*

The rich two-dimensional physics in a material with mechanical and chemical robustness makes graphene an intriguing platform for leveraging exotic low-dimensional phenomena for advanced functionality.[1−6] Recent advances in large-area chemical vapor deposition growth and transfer to arbitrary substrates now allow for fabrication of wafer-scale graphene device arrays.[7,8] Experimental observation, and ultimately practical implementation of the unique phenomena associated with massless Dirac fermions in graphene, however, is difficult and often requires a suite of sophisticated instrumentation.[3−6] Furthermore, due to its zero-gap nature, even the most mundane exploitation of graphene as a high-mobility channel in conventional field-effect transistors (FETs) is limited.[2] Interfacing graphene with complex oxides such as ferroelectrics may lead to new means of manipulating carriers in graphene and thus facilitate utilization of its promising electronic properties in devices.

Ferroelectric oxide thin films are suitable for high-speed nonvolatile memories, high-density capacitors, and advanced low-power logic elements due to their high susceptibility and large, electric-field controllable remanent polarization.[9−12] Recent developments in the synthesis of complex oxide thin films allow for nanometer-scale artificial structures compatible with low-power semiconductor technology.[13−16] Previous studies of graphene incorporated into FETs with ferroelectric gates have revealed a strong interaction between the gate dielectric and graphene leading to potentially useful attributes such as stable hysteresis curves or nonvolatility.[17−24] However, the observed characteristics of graphene on ferroelectric oxides have been attributed to extrinsic charging effects rather than a direct coupling of the ferroelectric polarization to charge carriers in graphene.[17−20] Similar hysteresis effects, extensively studied in graphene and carbon nanotube devices on nonferroelectric substrates, have been shown to be caused by relatively slow interactions with surrounding molecules such as H_2O and O_2,[25−28] charge injection into interfacial trap states,[29−31] and/or charge redistribution within the substrate caused by mobile and trapped charges.[32] In ambient air, these extrinsic factors result in a hysteresis between two p-type states for electric field or gate voltage cycles. Upon application of a positive gate voltage, the system exhibits enhanced p-doping, corresponding to a *positive* shift of the Dirac point in the transfer characteristics (drain current I_D versus gate voltage V_G curve). This behavior is the opposite of what is expected if direct coupling of the ferroelectric polarization and charge carriers in graphene existed. In this latter case, poling the ferroelectric in an “up” state (with the polarization pointing toward the graphene) should stabilize electrons in the graphene (making it n-type or at least less p-type) while poling the ferroelectric in the “down” state (with the polarization pointing away from the graphene) should stabilize holes (making the graphene more p-type). In other words, the electric field from the up-polarized $PbZr_{0.2}Ti_{0.8}O_3$ should create a positive offset in V_G leading to the Dirac point shifting to a more *negative*, rather than a more positive value. Extrinsic hysteresis effects opposing the ferroelectric polarization and the delayed response associated with slow motion of adsorbed molecules are undesirable aspects that complicate our understanding of graphene/ferroelectric interactions and therefore currently limit the applicability of this system.

Here, we report how contributions from surface/interface charging and adsorbed molecules can be separated from the

Received: January 16, 2013
Revised: March 5, 2013
Published: March 18, 2013

 © 2013 American Chemical Society

intrinsic interaction and how they can be sufficiently reduced to allow observation of direct effects of ferroelectric polarization on single-layer graphene. Stable and reversible ferroelectric operation in both capacitor and FET modes is shown with graphene/$PbZr_{0.2}Ti_{0.8}O_3$ hybrid structures. A complete reversal of the direction of the hysteresis in the transfer characteristics allows for reversible and permanent switching of the resistance state of the graphene channel. A conversion from p- to n-type in graphene/$PbZr_{0.2}Ti_{0.8}O_3$ FETs is shown with fast gate voltage sweeps or pulsed gate voltages.

Single-layer graphene with low defect density was grown on ultrapure Cu foils similar to "recipe B" of ref 8. Following chemical vapor deposition growth, the graphene films were transferred to the desired substrates using a one-touch wet transfer method that allows for Cu etching, washing, and deposition onto target substrates all in one bath designed for continuous flow of different solutions. Atomic force microscopy and Raman spectroscopy studies of graphene transferred to SiO_2 using this method revealed a minimum amount of polymer residue after transfer, continuous coverage, and low average defect densities as indicated by a low D to G peak intensity ratio <0.06 [Supporting Information, Figure S1]. The 2D to G peak intensity ratio of 3.02 with the G-band peak position of 1585.6 cm^{-1} as well as the 2D bandwidth Γ_{2D} = 26.8 cm^{-1} are indicative of single layer graphene.[33] As discussed in the Supporting Information, the one-touch transfer process developed here improved the coupling between graphene and the ferroelectric thin film, which is necessary to minimize the external charging effects observed previously. For device fabrication, the graphene films were transferred onto pulsed-laser deposition grown 140 nm $PbZr_{0.2}Ti_{0.8}O_3$/60 nm $SrRuO_3$/$SrTiO_3$ (001) heterostructures,[34] which were thoroughly cleaned before transfer without allowing the films to be exposed to air between cleaning and graphene deposition. Two types of devices were fabricated, capacitors and FETs, both with Pd as the contact metal for the graphene. Details of graphene and oxide growth, one-touch wet transfer method, and device fabrication can be found in the Supporting Information.

Using the capacitor structure, a robust ferroelectric response of the $PbZr_{0.2}Ti_{0.8}O_3$ film can be seen in the Pd/graphene/$PbZr_{0.2}Ti_{0.8}O_3$/$SrRuO_3$ capacitors with a coercive field of ~174 kV cm^{-1} (~2.44 V coercive voltage) [Figure 1a]. As a point of comparison, the hysteresis loop for a Pd top contact capacitor without graphene is also shown [Figure 1a]. Symmetric leakage current [Supporting Information Figure S2], square and symmetric hysteresis loops, negligible polarization offsets, and similar coercive fields are seen in the control capacitor. A noticeable difference is the smaller remanent ferroelectric polarization of the Pd/graphene/$PbZr_{0.2}Ti_{0.8}O_3$ structures (~23 μC cm^{-2} versus ~80 μC cm^{-2} in the control), which can be explained by the lower carrier density of the graphene being unable to compensate the polarization completely. Similar results have been shown in ferroelectric capacitors with semiconducting contacts.[35] A complete compensation of the remanent polarization would require a carrier density of about 5×10^{14} cm^{-2}, an enormous number for single-layer graphene. Graphene covered by a ferroelectric polymer film has also been shown to be unable to supply a sufficient number of carriers for complete compensation.[24] Another possible explanation for the reduced polarization is the existence of a dielectric layer at the interface of the graphene and $PbZr_{0.2}Ti_{0.8}O_3$ films, possibly caused by molecules such as

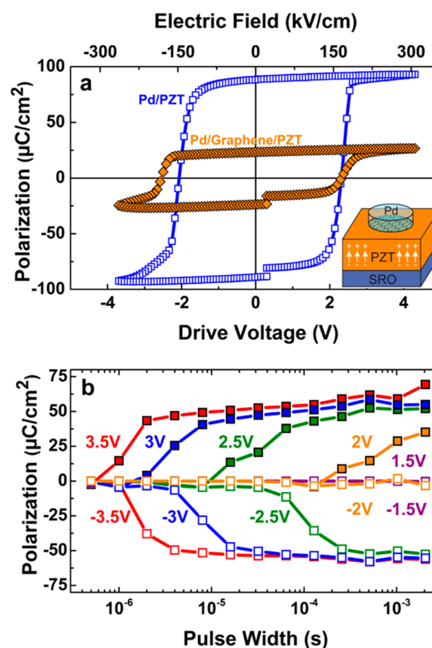

Figure 1. (a) Ferroelectric hysteresis loops of the $PbZr_{0.2}Ti_{0.8}O_3$ (PZT) film with Pd and graphene/Pd top contacts (blue open squares and orange-filled diamonds, respectively) with a frequency of 10 kHz. (b) Positve up negative down (PUND) switching measurements for a Pd/graphene/$PbZr_{0.2}Ti_{0.8}O_3$ capacitor as a function of pulse width for various pulse voltages. The ferroelectric polarization can be switched completely for positive and negative voltages with pulse durations of 0.008, 0.032, and 0.51 ms for applied voltages of 3.5, 3, and 2.5 V, respectively.

H_2O present on the surface of the $PbZr_{0.2}Ti_{0.8}O_3$ prior to or during the transfer process.[36]

Figure 1b shows the voltage magnitude and the pulse-width dependence of $PbZr_{0.2}Ti_{0.8}O_3$ polarization in the capacitors with Pd/graphene contacts. Fast ferroelectric polarization switching can be achieved in these capacitors. For a complete polarization reversal, pulse durations of 0.008, 0.032, and 0.51 ms are required for applied voltages of ±3.5, ± 3, and ±2.5 V, respectively. These results provide the necessary information to understand the time- and gate-voltage-dependent response of graphene FETs on $PbZr_{0.2}Ti_{0.8}O_3$. Fast and low-voltage responses may be particularly useful for manipulating electron transport in graphene with ferroelectric gates.

Having established ferroelectric polarization switching of $PbZr_{0.2}Ti_{0.8}O_3$ using graphene-based electrodes, we now consider a FET geometry with a graphene channel and a ferroelectric gate. The device structure [Figure 2a inset] includes an insulating SiO_2 layer to ensure low leakage current between the gate electrode and metal contact pads. For gate voltages not exceeding the coercive voltage of the $PbZr_{0.2}Ti_{0.8}O_3$ film, these devices exhibit transfer characteristics similar to graphene FETs on Si/SiO_2 substrates, further verified through gate-dependent Raman G-band peak position shift [Supporting Information Figure S3]. Because of the large dielectric constant of $PbZr_{0.2}Ti_{0.8}O_3$, a very small V_G range is necessary to effectively tune the carrier concentration. The Dirac point is typically at a slightly positive V_G (i.e., p-doped much like graphene on Si/SiO_2 substrates measured under air ambient) and the field-effect mobility is in the range of 200–1300 cm^2 V^{-1} s^{-1}. A possible reason for this reduced mobility in the graphene channel compared to devices fabricated similarly

dx.doi.org/10.1021/nl4002052 | Nano Lett. 2013, 13, 1693–1698

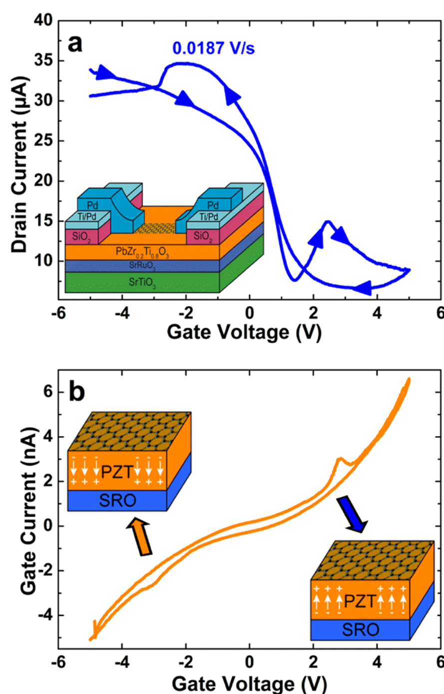

Figure 2. (a) Complex I_D-V_G characteristic for large gate voltages with a drain voltage of 50 mV and a gate voltage sweep rate of 0.0187 V/s. Inset: Schematic of a graphene transistor on $PbZr_{0.2}Ti_{0.8}O_3$. (b) Gate current measured simultaneously to (a). Note the different scales for drain and gate current. The gate current was always equal to or less than 0.1% of the drain current. Insets: Schematics of the ferroelectric polarization for different gate voltage regimes.

on Si/SiO$_2$ (typical mobility of 4000−10 000 cm^2 V^{-1} s^{-1}) is the strong graphene-substrate interaction, which has been shown to reduce carrier mobility.[37]

A more complex behavior, however, is observed when V_G exceeds the coercive field [Figure 2a]. Starting from $V_G = -5$ V, which causes the $PbZr_{0.2}Ti_{0.8}O_3$ to be poled "down" (i.e., polarization direction shown in the upper left inset of Figure 2b), sweeping V_G toward more positive values with a relatively slow sweep rate of 0.0187 V/s for this particular case reveals that the drain current (I_D) of this device reaches a minimum at $V_G = 1.36$ V, the Dirac point. As V_G becomes more positive, I_D starts to deviate from the "V-shape" of ambipolar behavior expected for a graphene FET with nonferroelectric gate dielectric. At $V_G \approx 2.5$ V, I_D shows a pronounced maximum followed by a strong decrease. In the reverse sweep, the Dirac point lies at ∼3.4 V. This shift in the Dirac point is indicative of strongly enhanced p-doping. At $V_G \approx 2.5$ V, another maximum followed by a rapid decrease in I_D is observed. Given that these nonmonotonic points in the I_D-V_G characteristics at $V_G = \pm 2.5$ V match the independently determined coercive fields of $PbZr_{0.2}Ti_{0.8}O_3$ (as shown in Figure 1a), we suggest that the polarization reversal in the ferroelectric film is responsible for the sudden drops in I_D and the shift in the Dirac point. This conclusion is further validated through multiple sweeps in the same direction [Supporting Information Figure S4] and the gate leakage current (I_G) behavior [Figure 2b] where precisely at the nonmonotonic points in I_D (at $V_G = \pm 2.5$ V) there are increases in $|I_G|$ corresponding to the polarization switching up (down) for positive (negative) V_G. These results are also similar

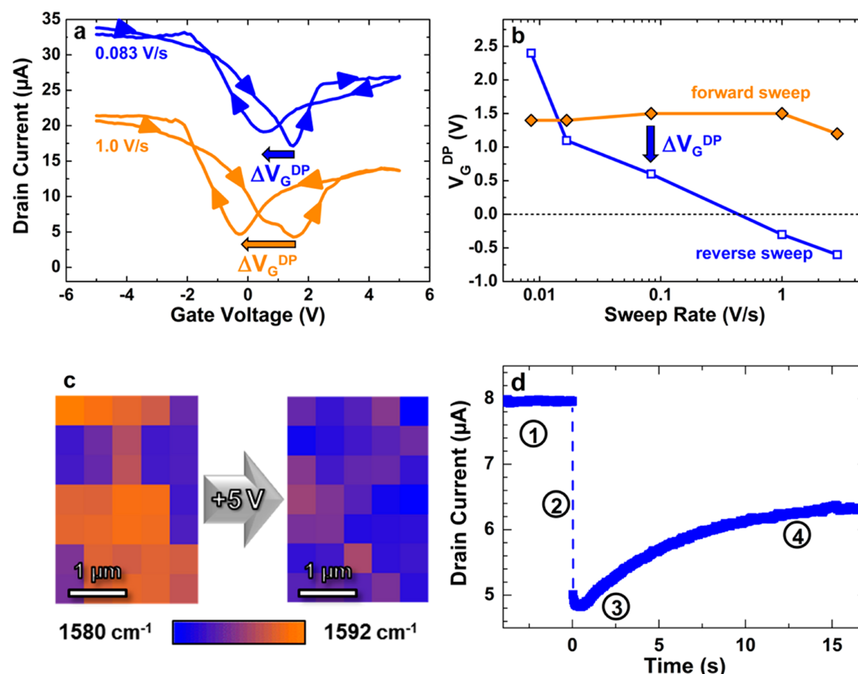

Figure 3. (a) Complex I_D-V_G characteristics of another graphene/$PbZr_{0.2}Ti_{0.8}O_3$ transistor for gate voltage sweeps past the $PbZr_{0.2}Ti_{0.8}O_3$ coercive voltage for two representative sweep rates as indicated and offset for clarity. (b) Sweep-rate dependent position of the current minima defined as the Dirac point voltage V_G^{DP} in the forward (orange, filled diamonds) and reverse sweep (blue, open squares). The dotted line represents zero gate voltage and separates the regimes of n- and p-doping. (c) Raman G-band position maps for a graphene transistor after gate sweeps ending at −5 V (left) and +5 V (right) with a gate voltage sweep rate of 0.046 V/s. (d) Current evolution before (regime 1) and after a 1 ms gate voltage pulse of +5 V at $t = 0$ s (regime 2) for another graphene/$PbZr_{0.2}Ti_{0.8}O_3$ transistor. The source−drain−current goes through a minimum corresponding to the Dirac point for this particular device (regime 3) before reaching a new equilibrium state (regime 4). The current is monitored through integration over 40 ms for each data point, making the pure gate-effect during the pulse indiscernible.

to recently observed I_G response of carbon nanotube network transistors with ferroelectric polymer gate insulators.[38]

While the simultaneous rise in $|I_G|$ with the drop in I_D is expected at the coercive voltages where the reversal of ferroelectric polarization occurs, the direction of the shift of the Dirac point and therefore the direction of the hysteresis requires further consideration. Enhanced p-doping (positive shift of the Dirac point) upon switching the polarization up with positive V_G is in agreement with previous experimental results for graphene[17,19] and CNT[39] based ferroelectric hybrid devices. However, as discussed in the introduction, this hysteresis cannot be caused directly by the ferroelectric polarization and therefore must be explained by extrinsic charging effects. This interpretation is experimentally supported in two ways. The first set of evidence comes from the changing behavior of graphene with V_G sweep rate. Transfer characteristics reveal that faster sweep rates actually lead to a reduction in the p-doping of the graphene and can even lead to n-doping as shown for the case of the sweep rate = 1 V/s [Figure 3a]. The V_G sweep rate dependence of the Dirac point shift (ΔV_G^{DP}) [Figure 3b] may then be explained by time-dependent charging/discharging or charge redistribution effects at the graphene/$PbZr_{0.2}Ti_{0.8}O_3$ interface. We note that for nonferroelectric gate dielectrics, increasing V_G sweep rate can only reduce the hysteresis associated with the positive ΔV_G^{DP}.[31] This is a distinctly different behavior than that observed for our graphene on ferroelectric $PbZr_{0.2}Ti_{0.8}O_3$ gate where the hysteresis is first transposed to the reverse direction, then the magnitude of the hysteresis *increases* with further increase in sweep rate [Figure 3b].

The second set of evidence for extrinsic charging/molecular adsorption effects complicating the observed hysteresis in the transfer curves of graphene FETs on $PbZr_{0.2}Ti_{0.8}O_3$ lies in the spatial inhomogeneity of charge distribution. Switching the polarization of $PbZr_{0.2}Ti_{0.8}O_3$ from "down" to "up" poled at a sweep rate of 0.046 V/s leads to a reduction in p-doping as verified by the net decrease in Raman G-band position to a nearly intrinsic level [Figure 3c]. However, local variations in the G-band position for both the "up" and "down" poled cases are indicatives of charge inhomogeneities. These variations in charge density are reminiscent of "charge puddles" that have been associated with spatial distribution of the surface potential on nonferroelectric substrates supporting the graphene layer.[40,41] This spatial inhomogeneity also manifests itself in a small, plateau-like shoulder in the transfer curves close to the Dirac point resulting from different regions of the graphene channel reaching minimum conductance at different gate voltages [forward sweep in the bottom curve in Figure 3a for $V_G \approx 1$ V]. Similar behavior in the transfer characteristics has been shown to arise when local doping levels have been intentionally varied by charge injection into graphene/oxide interface trap states in a previous study.[42]

Given that both ferroelectric polarization and variations in local charge density through adsorbed molecules can contribute to the observed ferroelectric-gated graphene FET characteristics, we now discuss the time evolution of I_D upon polarization switching using a voltage pulse [Figure 3d]. The polarization of the $PbZr_{0.2}Ti_{0.8}O_3$ film is reversed using a short V_G pulse while I_D is monitored at a small applied drain voltage V_D of 50 mV. A 1 ms V_G pulse is applied at $t = 0$ and a sufficiently large voltage (5 V) is used to ensure complete switching of the polarization. The graphene starts in a p-type state (region 1). Following the gate pulse, I_D drops instantaneously (region 2). On the basis of the sweep-rate dependence, we expect the graphene to be slightly n-type at this stage. After the initial fast drop, I_D shows a slower response going through a minimum corresponding to the Dirac point at $t \sim 0.5$ s (region 3) and then increasing to reach an equilibrium value (region 4). The final value of I_D corresponds to a net reduction in p-doping of graphene with respect to the initial state. The initial fast I_D drop is mainly in response to the ferroelectric polarization change. The slow change may be attributed to reconfiguration of polar molecules at the interface that can (1) partially screen the polarization field of the ferroelectric and (2) cause charge redistribution between graphene, adsorbed molecules, and/or interface trap states. Despite the opposing slow molecular/interface effects, the final switched state of graphene remains nonvolatile (Supporting Information Figure S6).

The presence of opposing hysteresis mechanisms (ferroelectric polarization vs molecular/interface effects) in our hybrid structures can be utilized to achieve a broader range of carrier densities (and type) in graphene to be accessible. To demonstrate this ability, we compare the response of graphene FETs measured in air and in vacuum ($<3 \times 10^{-7}$ Torr) after annealing at 110 °C for several hours to reduce the number of adsorbed molecules. Figure 4a shows the transfer characteristics of a graphene FET under different conditions. These curves are

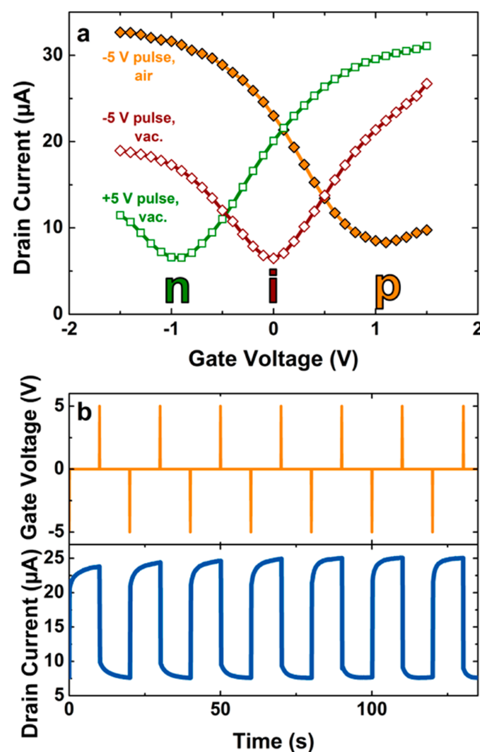

Figure 4. (a) Small gate voltage sweeps not exceeding the coercive voltage measured after 1 ms gate voltage pulses. p-type, nearly intrinsic, and n-type behavior can be observed after a −5 V pulse in air (orange, filled diamonds), a −5 V pulse in vacuum (red, open diamonds), and a +5 V pulse in vacuum (green, open squares), respectively. (b) Multiple gate voltage pulses applied to a similar device in air (upper panel) and resulting reversible and reproducible switching between a highly p-doped state for the down-polarized state and a nearly intrinsic level for the up-polarized case. The current is monitored through integration over 100 ms for each data point, making the pure gate-effect during the pulse indiscernible.

measured within a small gate voltage range, well below the coercive voltage of the $PbZr_{0.2}Ti_{0.8}O_3$ film, after 1 ms gate voltage pulses to switch the ferroelectric polarization. After a −5 V pulse in air, switching the polarization down, the graphene is p-doped with the Dirac point at $V_G \approx 1$ V. The positive value of the Dirac point and therefore the graphene being p-type can be attributed to a combination of doping due to the ferroelectric polarization, extrinsic effects of polar molecules, and charge trapping in the interface states. Performing the same operation in vacuum, the graphene channel is now nearly intrinsic (Dirac point at $V_G \approx 0$ V), which has to be attributed to the combination of the ferroelectric polarization and interfacial trap states after the (partial) removal of polar molecules through the vacuum heat treatment. A positive 5 V V_G pulse in vacuum, switching the polarization up, completely converts the graphene to n-type (Dirac point at $V_G \approx -1$ V), demonstrating that the switching of the ferroelectric polarization, rather than extrinsic effects of adsorbed molecules, dictate the carrier type and density. The shift in the Dirac point from $V_G = 1$ V on a down-polarized $PbZr_{0.2}Ti_{0.8}O_3$ film in air to $V_G = -1$ V on an up-polarized $PbZr_{0.2}Ti_{0.8}O_3$ film in vacuum corresponds to an impressively large change in carrier density/type from $\sim 6 \times 10^{12}$ holes/cm^2 to $\sim 6 \times 10^{12}$ electrons/cm^2. The switching process utilizing pulsed gate voltages can be used both in vacuum and in air to switch reversibly and permanently between high- and low-conductance states, corresponding to the graphene switching between n-type and intrinsic in vacuum and p-type and intrinsic in air. Devices can be switched reliably at least several thousands of times [Figure 4b and Supporting Information Figure S7].

In conclusion, with an improved transfer and fabrication process we have demonstrated that graphene can reversibly switch the ferroelectric polarization of a $PbZr_{0.2}Ti_{0.8}O_3$ thin film and the ferroelectric polarization can in turn control the carrier type and density in graphene FETs. One of the most striking consequences of ferroelectric polarization switching dominating electron transport in graphene is the complete reversal of the hysteresis direction. The positive shift of the Dirac point with positive gate voltages, which is usually observed in graphene on nonferroelectric substrates including the most commonly used SiO_2, has been attributed to adsorbed molecules such as H_2O and O_2 enhancing charge trapping at the interface.[25−28] The same hysteresis direction has also been observed on ferroelectric oxide substrates until now because these extrinsic molecular effects rather than the actual ferroelectric polarization dictate the response of graphene. These extrinsic effects should be caused by slow molecular motion or oxidation/reduction reactions and therefore we have been able to enhance direct ferroelectric gate effect on graphene either by fast voltage sweeps or voltage pulses and an optimized fabrication process, enabling reversible and nonvolatile operation. Furthermore, we have demonstrated that a complete conversion of a p-type graphene into n-type through ferroelectric polarization change is possible by controlling the extrinsic molecular effects. This demonstration of strong influence of ferroelectric polarization on the electronic properties of graphene opens new routes toward manipulating this unique 2D electron system.

■ ASSOCIATED CONTENT

Supporting Information

Graphene growth and transfer, pulsed laser deposition of ferroelectric thin films, transistor and capacitor fabrication, Raman spectrum acquisition and fitting, leakage characterization of the $PbZr_{0.2}Ti_{0.8}O_3$ film with and without graphene, initial characterization of FET structure (transfer characteristics and gate-dependent Raman measurement), multiple FET gate voltage sweeps in the same direction, comparison of transfer methods for device characteristics and retention and reversibility measurements. This material is available free of charge via the Internet at http://pubs.acs.org.

■ AUTHOR INFORMATION

Corresponding Author

*E-mail: (L.W.M.) lwmartin@illinois.edu; (M.S.) mshim@illinois.edu.

Author Contributions

The manuscript was written through contributions of all authors. All authors have given approval to the final version of the manuscript.

Notes

The authors declare no competing financial interest.

■ ACKNOWLEDGMENTS

The authors would like to acknowledge the support of the National Science Foundation and the Nanoelectronics Research Initiative under Grants DMR-1124696 and DMR-09-05175. C.B. and L.W.M. acknowledge support from the Army Research Office under Grant W911NF-10-1-0482. Experiments were partially carried out in the Materials Research Laboratory Central Facilities, University of Illinois.

■ ABBREVIATIONS

PZT, $PbZr_{0.2}Ti_{0.8}O_3$; FET, field-effect transistor

■ REFERENCES

(1) Geim, A. K.; Novoselov, K. S. *Nat. Mater.* **2007**, *6*, 183−91.
(2) Castro Neto, A. H.; Peres, N. M. R.; Novoselov, K. S.; Geim, a. K. *Rev. Mod. Phys.* **2009**, *81*, 109−162.
(3) Zhang, Y.; Tan, Y.-W.; Stormer, H. L.; Kim, P. *Nature* **2005**, *438*, 201−4.
(4) Bolotin, K. I.; Ghahari, F.; Shulman, M. D.; Stormer, H. L.; Kim, P. *Nature* **2009**, *462*, 196−9.
(5) Katsnelson, M. I.; Novoselov, K. S.; Geim, a. K. *Nat. Phys.* **2006**, *2*, 620−625.
(6) Novoselov, K. S.; Geim, A. K.; Morozov, S. V; Jiang, D.; Katsnelson, M. I.; Grigorieva, I. V; Dubonos, S. V; Firsov, A. A. *Nature* **2005**, *438*, 197−200.
(7) Li, X.; Cai, W.; An, J.; Kim, S.; Nah, J.; Yang, D.; Piner, R.; Velamakanni, A.; Jung, I.; Tutuc, E.; Banerjee, S. K.; Colombo, L.; Ruoff, R. S. *Science* **2009**, *324*, 1312−4.
(8) Huang, P. Y.; Ruiz-Vargas, C. S.; Van der Zande, A. M.; Whitney, W. S.; Levendorf, M. P.; Kevek, J. W.; Garg, S.; Alden, J. S.; Hustedt, C. J.; Zhu, Y.; Park, J.; McEuen, P. L.; Muller, D. a *Nature* **2011**, *469*, 389−92.
(9) Schlom, D. G.; Guha, S.; Datta, S. *MRS Bull.* **2008**, *33*, 1017−1025.
(10) Scott, J. F. *Science* **2007**, *315*, 954−9.
(11) Setter, N.; Damjanovic, D.; Eng, L.; Fox, G.; Gevorgian, S.; Hong, S.; Kingon, A.; Kohlstedt, H.; Park, N. Y.; Stephenson, G. B.; Stolitchnov, I.; Taganstev, A. K.; Taylor, D. V.; Yamada, T.; Streiffer, S. *J. Appl. Phys.* **2006**, *100*, 051606.
(12) Dawber, M.; Scott, J. F. *Rev. Mod. Phys.* **2005**, *77*, 1083−1130.
(13) Ahn, C. H.; Rabe, K. M.; Triscone, J.-M. *Science* **2004**, *303*, 488−91.
(14) Schlom, D. G.; Chen, L.-Q.; Eom, C.-B.; Rabe, K. M.; Streiffer, S. K.; Triscone, J.-M. *Annu. Rev. Mater. Res.* **2007**, *37*, 589−626.

(15) Martin, L. W.; Chu, Y.-H.; Ramesh, R. *Mater. Sci. Eng. R* **2010**, *68*, 89−133.
(16) Lee, W.; Han, H.; Lotnyk, A.; Schubert, M. A.; Senz, S.; Alexe, M.; Hesse, D.; Baik, S.; Gösele, U. *Nat. Nanotechnol.* **2008**, *3*, 402−7.
(17) Hong, X.; Hoffman, J.; Posadas, a.; Zou, K.; Ahn, C. H.; Zhu, J. *Appl. Phys. Lett.* **2010**, *97*, 033114.
(18) Hong, X.; Posadas, a.; Zou, K.; Ahn, C.; Zhu, J. *Phys. Rev. Lett.* **2009**, *102*, 2−5.
(19) Song, E. B.; Lian, B.; Min Kim, S.; Lee, S.; Chung, T.-K.; Wang, M.; Zeng, C.; Xu, G.; Wong, K.; Zhou, Y.; Rasool, H. I.; Seo, D. H.; Chung, H.-J.; Heo, J.; Seo, S.; Wang, K. L. *Appl. Phys. Lett.* **2011**, *99*, 042109.
(20) Hsieh, C.-Y.; Chen, Y.-T.; Tan, W.-J.; Chen, Y.-F.; Shih, W. Y.; Shih, W.-H. *Appl. Phys. Lett.* **2012**, *100*, 113507.
(21) Zheng, Y.; Ni, G.-X.; Toh, C.-T.; Zeng, M.-G.; Chen, S.-T.; Yao, K.; Özyilmaz, B. *Appl. Phys. Lett.* **2009**, *94*, 163505.
(22) Ni, G.; Zheng, Y.; Bae, S.; Tan, C.; Kahya, O. *ACS Nano* **2012**, *6*, 3935−3942.
(23) Zheng, Y.; Ni, G.-X.; Toh, C.-T.; Tan, C.-Y.; Yao, K.; Özyilmaz, B. *Phys. Rev. Lett.* **2010**, *105*, 5−8.
(24) Raghavan, S.; Stolichnov, I.; Setter, N.; Heron, J.-S.; Tosun, M.; Kis, A. *Appl. Phys. Lett.* **2012**, *100*, 023507.
(25) Xu, H.; Chen, Y.; Zhang, J.; Zhang, H. *Small* **2012**, *8*, 2833−40.
(26) Kim, W.; Javey, A.; Vermesh, O.; Wang, Q.; Li, Y.; Dai, H. *Nano Lett.* **2003**, *3*, 193−198.
(27) Pascal-Levy, Y.; Shifman, E.; Pal-Chowdhury, M.; Kalifa, I.; Rabkin, T.; Shtempluck, O.; Razin, A.; Kochetkov, V.; Yaish, Y. *Phys. Rev. B* **2012**, *86*, 115445.
(28) Shim, M.; Back, J.; Ozel, T.; Kwon, K.-W. *Phys. Rev. B* **2005**, *71*, 205411.
(29) Lee, J. S.; Ryu, S.; Yoo, K.; Choi, I. S.; Yun, W. S.; Kim, J. *J. Phys. Chem. C* **2007**, *111*, 12504−12507.
(30) Radosavljević, M.; Freitag, M.; Thadani, K. V.; Johnson, A. T. *Nano Lett.* **2002**, *2*, 761−764.
(31) Wang, H.; Wu, Y.; Cong, C.; Shang, J.; Yu, T. *ACS Nano* **2010**, *4*, 7221−8.
(32) Robert-Peillard, A.; Rotkin, S. V. *IEEE Trans. Nanotechnol.* **2005**, *4*, 284−288.
(33) Kalbac, M.; Reina-Cecco, A.; Farhat, H.; Kong, J. *ACS Nano* **2010**, *4*, 6055−6063.
(34) Karthik, J.; Damodaran, A. R.; Martin, L. W. *Adv. Mater.* **2012**, *24*, 1610−5.
(35) Wurfel, P.; Batra, I. P. *Phys. Rev. B* **1973**, *8*, 5126−5133.
(36) Tagantsev, A. K.; Landivar, M.; Colla, E.; Setter, N. *J. Appl. Phys.* **1995**, *78*, 2623.
(37) Fratini, S.; Guinea, F. *Phys. Rev. B* **2008**, *77*, 195415.
(38) Choi, Y. S.; Sung, J.; Kang, S. J.; Cho, S. H.; Hwang, I.; Hwang, S. K.; Huh, J.; Kim, H.-C.; Bauer, S.; Park, C. *Adv. Funct. Mater.* **2012**, n/a−n/a.
(39) Paruch, P.; Posadas, a.-B.; Dawber, M.; Ahn, C. H.; McEuen, P. L. *Appl. Phys. Lett.* **2008**, *93*, 132901.
(40) Martin, J.; Akerman, N.; Ulbricht, G.; Lohmann, T.; Smet, J. H.; Von Klitzing, K.; Yacoby, a. *Nat. Phys.* **2007**, *4*, 144−148.
(41) Zhang, Y.; Brar, V. W.; Girit, C.; Zettl, A.; Crommie, M. F. *Nat. Phys.* **2009**, *5*, 722−726.
(42) Chiu, H.-Y.; Perebeinos, V.; Lin, Y.-M.; Avouris, P. *Nano Lett.* **2010**, *10*, 4634−9.